What Microseismicity Tells Us About Re-fracturing – An Engineering Approach to Re-fracturing Design

Alireza Agharazi, Sudhendu Kashikar

MicroSeismic, Inc.

ABSTRACT:

Microseismic monitoring of re-fracturing of depleted horizontal wells frequently shows a concentration of microseismic activity at the heel area when no mechanical isolation is used. This observation indicates a localized stimulation of the well at the heel area, which potentially leaves a considerable length of the well unstimulated toward the toe. Different completion techniques, ranging from injecting diverters to using mechanical intervention methods, are usually used to avoid the localized stimulation and to enhance the treatment effectiveness. However, often overlooked is the effect of the reservoir rock's mechanical characteristics on the treatment efficiency.

We studied the geomechanics of re-fracturing and ran a series of numerical simulations to investigate: i) the effect of pressure drop along the lateral, ii) diverter effectiveness, and iii) the possibility of creating new transverse fractures from new perforations. For common casing diameters and fracturing fluids the pressure drop along the lateral is high and can result in a considerable pressure contrast of a few thousand psi between the heel and the toe. This results in the dilation of pre-existing fractures at the heel under the higher injection pressures developed in that section. In the absence of effective diverters, this condition persists throughout the treatment and gives rise to localized stimulation of the well limited to the heel, as observed by the concentration of microseismic events toward the heel. Our study indicates that the dominant stimulation mechanism during the studied re-fracturing treatments was the shear slippage of natural fractures by a pore pressure-driven mechanism, as opposed to creation of new transverse fractures from the new perforations. This conclusion is consistent with the observed long delay in microseismic response to the treatment and also with the observed increasing trend of the treatment pressure with pumping cycles.

Based on these findings, we developed an alternative re-fracturing method that aims at increasing the reservoir effective complexity and enhancing the conductivity of the pre-existing hydraulic fractures uniformly along the well. The proposed method consists of a prolonged low-pressure and low-rate pad stage to pressurize the reservoir, followed by a high-pressure injection stage to stimulate natural fractures and place proppant in the new fractures. Critical to the success of this method is to avoid a high pressure contrast along the well, which can be achieved by proper selection of injection pressure and fluid viscosity with respect to the reservoir stresses and pressures along the well and the well characteristics. Numerical simulations indicate that the proposed method can considerably enhance the efficiency of re-fracturing treatments, at no additional cost compared to the common re-fracturing methods.

1 Introduction

Re-fracturing of horizontal wells is a simpler and often more economical alternative to drilling a new well to boost production from a declining well and enhance the ultimate recovery. These goals are achieved mainly by improving the reservoir-wellbore fluid connectivity and enhancing the reservoir drainage characteristics.

The main stimulation mechanisms during re-fracturing of horizontal wells are; Vincent (2010):

- Improvement of fracture conductivity either by restoring the lost conductivity due to proppant embedment and/or degradation, or by placing proppant in initially poorly propped sections.

- Enhancement of reservoir-fracture contact area either by adding new transverse/longitudinal fractures or enlarging pre-existing fracture geometry.
- Increase of productive complexity by stimulating fresh natural fractures/rocks or by re-energizing already stimulated fractures/rock.

In most re-fracturing treatments of horizontal wells, no mechanical stage isolation is used. The fluid is bullheaded, relying on diverting agents, usually sand slugs or ball sealers, added after each pumping cycle to move re-fracturing down the lateral. The main disadvantage of this method is lack of control on where the diverters sit along the lateral and which part of the well is benefiting from re-fracturing; Sudhendu and Jbeili (2015). When new perforations are added, reservoir pressure and stress heterogeneity along the well have a significant effect on whether fresh fractures are propagated from newly added perforations or pre-existing fractures, connected to the old perforations, are dilated. Because rock failure is governed by effective stresses, well sections with higher reservoir pressures are easier to break than the more depleted sections.

Lower apparent Instantaneous Shut-In Pressure (ISIP) and fracture gradient, compared to the original values, are usually observed during re-fracturing; Diakhate et al. (2015), Lanzet et al. (2007), Kashikar and Jbeili (2015). Diakhate et al. (2015) reported a 1,000–1,200 psi drop in ISIP for one re-fractured well and up to 3,000 psi reduction in the closure pressure for another re-fractured well. Given the increase of effective stresses during production which results in higher fracture gradients, the observed lower pressures during re-fracturing probably indicate the dominance of dilation of old fractures versus propagation of new fractures. This is an important factor when the economic viability of a re-fracturing treatment depends mainly on breaking the fresh rocks in the bypassed pay zones left after the initial treatments. This is usually the case in older wells where the initial stage lengths are long; Sudhendu and Jbeili, (2015) and Vincent (2010).

Another challenge to the efficiency and economic viability of re-fracturing in horizontal wells is the limited stimulation of the well that usually occurs closer to the heel when no mechanical isolation is used. Sudhendu and Jbeili (2015) showed the real-time microseismic data of two re-fractured wells, where all of the microseismic events were concentrated toward the heel, leaving about two-thirds of the laterals unstimulated.

In this paper, we examine the microseismic data from three re-fractured horizontal wells in two different plays. We also investigate the difference between microseismic response to fracturing and to re-fracturing by examining a case where both fracturing and re-fracturing were conducted simultaneously in two adjacent wells. The factors contributing to the concentration of microseismic events during re-fracturing are then discussed. Several numerical models were built to simulate the stress and pressure changes during production and re-fracturing of a horizontal well. These simulations along with geomechanical analyses provide insight into the stress and pressure change patterns during production and re-fracturing and how they impact the stimulation mechanism during re-fracturing. This study helps to explain the initially lower apparent ISIP during re-fracturing and why it increases as the treatment continues. Based on the microseismic observations and geomechanical simulations, we determine the dominant stimulation mechanism for the studied re-fracturing cases. Finally, an alternative re-fracturing method is presented that targets the improvement of pre-existing fractures' conductivity and enhancement of productive complexity. The efficiency of the proposed method is examined by numerical simulations.

2 Microseismic Observations of Re-fracturing

A study of microseismic data from several re-fractured horizontal wells show that the typical microseismic response to re-fracturing in most of these wells includes:

- The concentration of microseismic events towards the heel.
- A time lag of several hours between the start of pumping and the onset of microseismic activity.

These observations are not specific to any particular field or formations but are common in most of the studied wells. In none of the wells, however, any mechanical isolation was used. The fluid was bullheaded, relying on diverter agents, usually sand slugs or bio-balls, to divert the fluid down the lateral after each pumping stage.

Three re-fractured wells were chosen for more detailed studies; two in the Haynesville formation and one in the Eagle Ford formation. For each well, we investigated the final distribution of microseismic events and the timing of the events with reference to the onset of pumping. All three wells had been initially treated by hydraulic fracturing with average stage lengths of 250–300 ft and were produced for several months before being re-treated by re-fracturing. The total pumping time (excluding the pump break times) was 34 hours for well A, 42 hours for well B and 49 hours for well C. The pumping rate was between 60 and 70 bbl/min for all cases. The initial fracturing stage lengths range from 250 ft to 320 ft for all three wells.

Figure 1 shows the microseismic event counts versus cumulative injected slurry for the studied wells. In all cases, it took several hours of pumping (7–18 hours) before any microseismicity was recorded. The volume of slurry injected during this microseismically “silent” period ranged between 13,000 and 40,000 bbl.

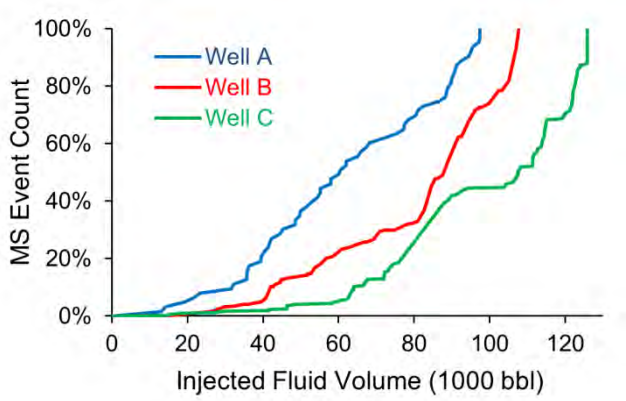

Figure 1: Microseismic event counts versus cumulative injected fluid volume. The volume of slurry injected during the microseismically silent period is 13,000 bbl for well A, 20,000 bbl for well B, and 40,000 for well C.

In another case study, microseismic data from two wells was used to compare the microseismic responses between re-fracturing and fracturing. These two wells were located in two adjacent pads that were monitored using the same surface geophone arrays and treated simultaneously. Both wells targeted the same pay zone at the same depth, so the effects of variations in the regional stresses and rock properties on the microseismic response are negligible.

Figure 2 shows the cumulative slurry and microseismic events versus time for four consecutive fracturing stages in well 1 (fracturing well). Figure 3 shows the same parameters for all stages of well 2 (re-fracturing well). During fracturing, the microseismic response is almost instantaneous with the onset of pumping; whereas during re-fracturing, it takes several hours of pumping and several thousand barrels of slurry before any microseismic event is observed.

Re-fracturing in Figure 1 and Figure 3 shows a progressive increase in event count per stage as the treatment continues. The last pumping stages in Figure 3 show considerably more events than the middle stages. The difference between the re-fracturing microseismicity and the initial fracturing microseismicity indicates the time dependency of the stimulation mechanism during re-fracturing.

This will be discussed further in Section 4: Geomechanics of Re-fracturing.

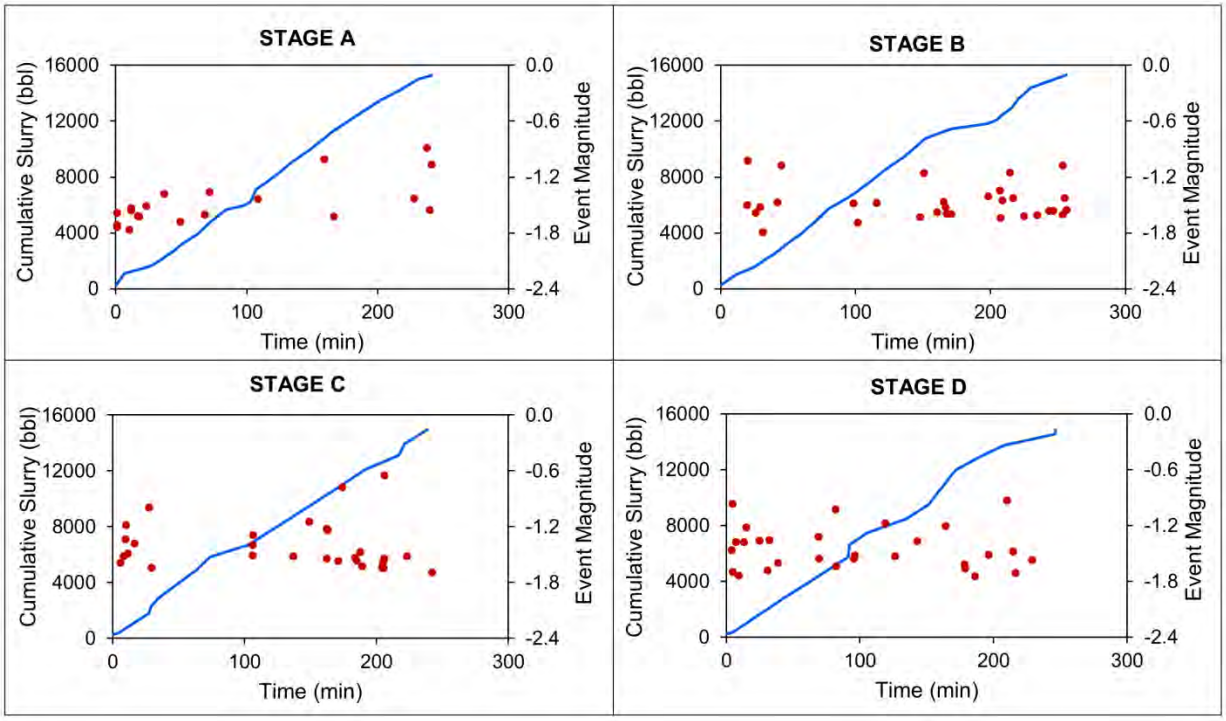

Figure 2: Cumulative slurry versus time graphs with microseismic event time sequence and magnitude for four consecutive fracturing stages in well 1. Average pumping rate is 65 bbl/min.

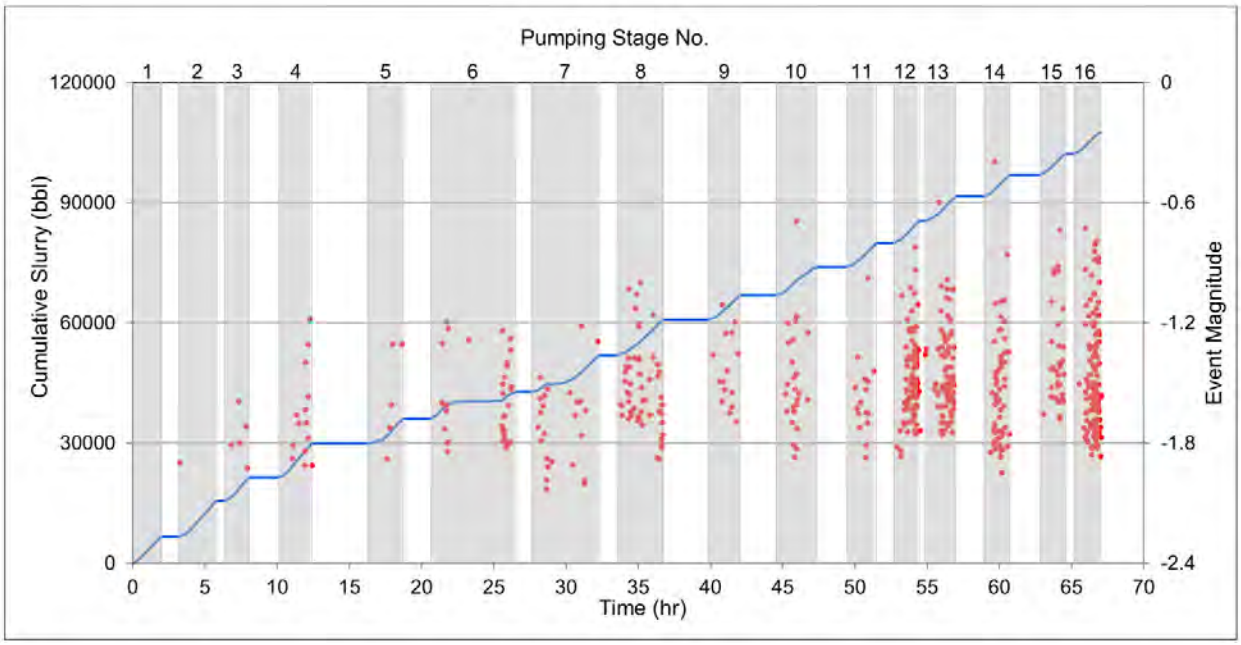

Figure 3: Cumulative slurry versus treatment time graphs with microseismic event time sequence and magnitudes for 16 stages of re-fracturing in well 2. Major microseismic events start after 7 hours of treatment and injection of about 20,000 barrels of slurry. Average pumping rate is 65 bbl/min.

Figure 4 shows the concentration of the microseismic events at the first 20–30% of the lateral length for the three re-fractured wells in the Haynesville and Eagle Ford formations. No microseismic events were recorded at the toe in any of these wells. It should be noted that surface geophone arrays were used for microseismic monitoring of these wells; therefore there is no event distribution bias toward the observation well, as might be the case if downhole microseismic monitoring was used.

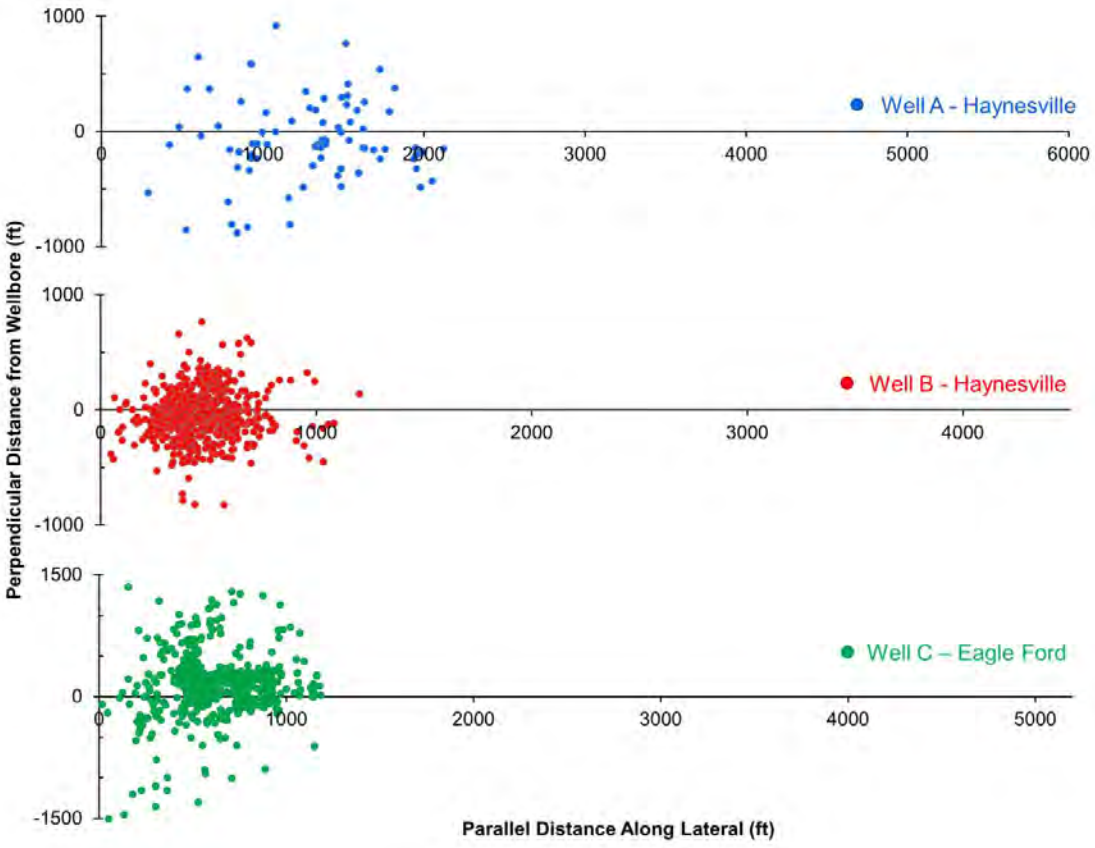

Figure 4: Distribution of microseismic events for the three horizontal wells in Haynesville and Eagle Ford. Pumping times were 36 hours for well A, 40 hours for well B, and 49 hours for well C (excluding pumping break times).

The localized stimulation of the wells at the heel, indicated by the high concentration of microseismic events, adversely affects the efficiency of re-fracturing by leaving a considerable length of the laterals unstimulated. The next section discusses the two important factors contributing to this effect.

3 Localized Stimulation at the Heel

Our assessment of the pump data and microseismic events indicates that when no mechanical isolation is used the cumulative effect of the following two factors results in the concentration of microseismic events toward the heel:

i. Pressure drop along the lateral due to frictional forces, which causes a high pressure contrast between the heel and the toe, during the treatment
ii. Inefficiency of diverters in diverting the fluid along the lateral after each pumping cycle.

To further investigate these effects, a generic numerical model of re-fracturing was constructed and several simulations were performed. A three-dimensional finite difference code, which allows modeling of the coupled fluid-mechanical problems, was used for these simulations. The model included a pressure-drop function that constantly calculated the frictional losses and updated the pressure profile along the lateral on a real-time basis throughout the simulations. A multi-stage re-fracturing treatment was simulated, assuming two extreme cases: fully effective diverters and non-effective diverters. The synthetic microseismic events were monitored and plotted during the simulations and used as a means to demonstrate the effect of diverters.

3.1 Numerical Simulation – Model Setup

The numerical model represents a 6,400-ft lateral with 61 perforations, including thirty-one old perforations and thirty new perforations. Each new perforation was added between two consecutive old perforations, reducing the initial perforation spacing from 206 ft to 103 ft.

A normal faulting stress regime (S_v>S_{Hmax}> S_{hmin}) was applied in the model, with the minimum horizontal stress (S_{hmin}) direction parallel to the lateral. Gravitational stresses were initialized assuming a rock density of 2,600 kg/m^3. At each depth, the horizontal stresses were calculated as a fraction of vertical stress, assuming S_{Hmax}=0.8S_v, and S_{hmin} = 0.8S_{Hmax}. A hydrostatic pore pressure distribution was considered in the model.

To address the effect of production on pore pressure and reservoir stresses, reservoir pressure was reduced around the pre-existing fractures connected to the old perforations. For the sake of simplicity, a similar depletion pattern was repeated for all the old perforations along the lateral. The maximum depletion ratio was taken equal to 15% at the well location, which reduces logarithmically with distance from the well (Figure 5). The depleted reservoir stresses were calculated by bringing the model to equilibrium after applying the depleted pressures.

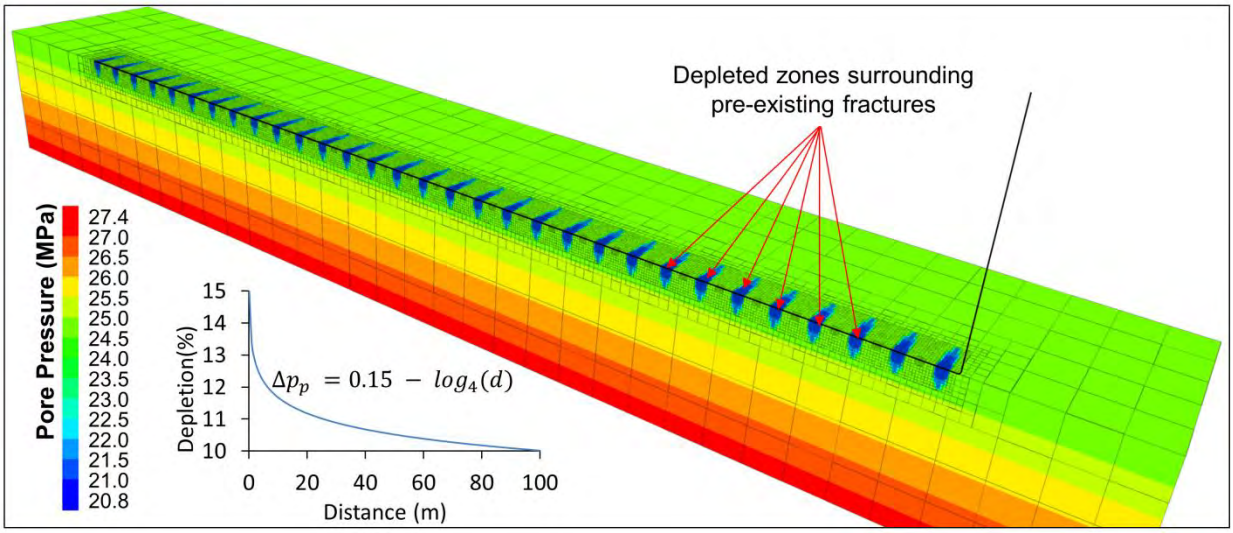

Figure 5: Pore pressure contours and depleted zones around pre-existing hydraulic fractures. Reservoir pressure depletion follows a logarithmic function of distance with the maximum depletion ratio of 15% at the lateral. The lateral extends 6,400 ft and includes 31 old perforations (206 ft apart) and 30 new perforations, added between the old ones, reducing the perforation distance to 103 ft for re-fracturing.

A background DFN, consisting of two sub-vertical fracture sets, perpendicular to each other, was populated in the model (Figure 6). Shear slippage on these fractures was monitored during the simulations and any failure was recorded as a synthetic microseismic event.

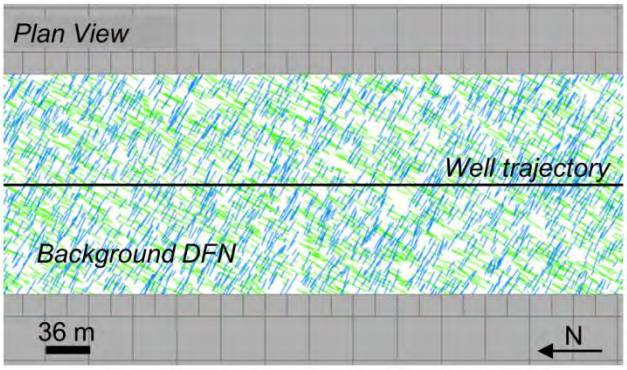

Figure 6: Horizontal section at the well depth showing the background DFN in the numerical models. Set 1 (blue): 90° / 30°±5 (dip/dip direction) and Set 2 (green): 90° / 120°±5 (dip/dip direction)

3.2 Pressure Drop Calculation Along Lateral

When bullheading re-fracturing into a long lateral, the pressure losses due to frictional forces result in a considerable pressure contrast between the heel and the toe. For the common lateral lengths of 5,000–7,500 ft, the pressure contrast can be as high as a few thousand psi for a slick water treatment. The pressure drop is a function of pumping rate, fluid viscosity, casing diameter, and the casing inner wall roughness. Pumping rate and fluid viscosity can be adjusted to lower the pressure drop rate during the treatment. Adding friction reducers can also considerably reduce the frictional forces during a slick water treatment. Due to discharge from perforations, the pressure drop rate is not constant along the lateral, but depends on the flow rate between each consecutive pair of perforations, as shown in Figure 7.

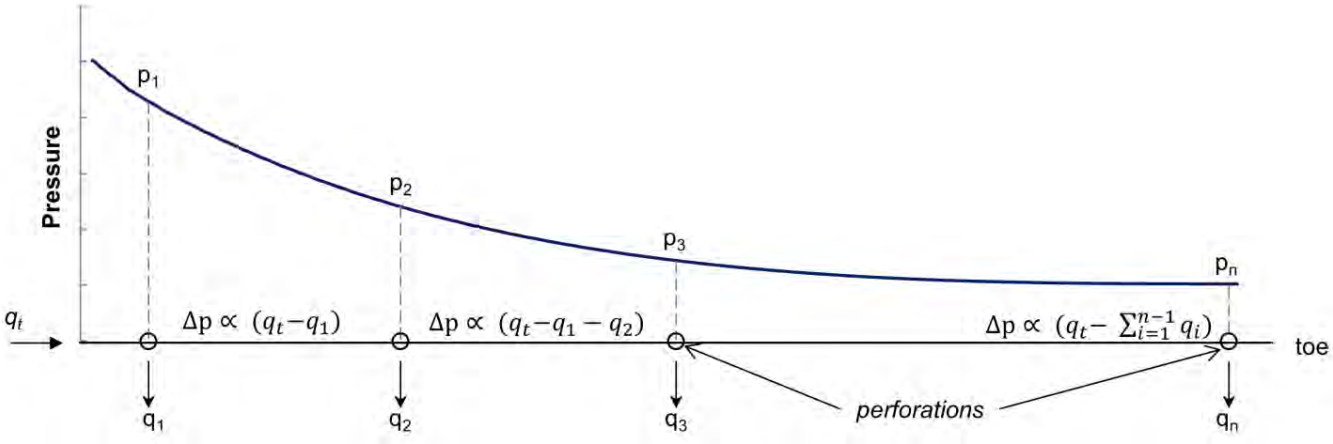

Figure 7: Schematic pressure profile along a horizontal well during re-fracturing. The pressure drop rate is not constant along the lateral due to discharge from perforations (q_i). The actual flow rate between two consecutive perforations is calculated by considering the discharge from perforations

The pressure drop can be calculated using the Darcy-Weisbach Equation, as follows; Munson et al. (2012):

$$\Delta p = f \times \frac{L}{D} \times \frac{\rho}{2} \times v^2 \qquad (1)$$

where:

Δp: pressure drop

f: pipe friction coefficient

L: well length

D: well diameter

ρ: fluid density

v: flow velocity

The pipe friction coefficient can be calculated from the following equations for laminar and turbulent flow, respectively:

$$f = \frac{64}{R_e} \quad \textit{(For laminar flow)} \qquad (2)$$

$$\frac{1}{\sqrt{f}} = -2log_{10}\left(\frac{e}{3.7\,D} + \frac{2.51}{R_e\sqrt{f}}\right) \textit{(For turbulent flow)} \qquad (3)$$

where R_e is the Reynolds number and e is the roughness height of the casing in the unit of length.

Equation (3) is known as the Colebrook-White Equation and applies when $R_e > 4{,}000$. Considering the common casing sizes (4½ inch) and injection rates for re-fracturing (>50 bbl/min), the flow is always turbulent; therefore, Equation (3) can be used. The casing friction coefficient can also be estimated from the Moody chart; Munson et al. (2012). The Reynolds number is calculated from the following equation:

$$R_e = \frac{\rho v D}{\mu} \qquad (4)$$

where ρ is fluid density and μ is fluid dynamic viscosity.

For a common casing diameter of 4½ inches, the pressure drop rate along the lateral can reach as high as 0.6–0.9 psi/ft, depending upon the casing roughness ($e = 0 - 0.1$ mm), at the flow rate of q = 60 bbl/min for a slick water treatment ($\mu = 2.5$ cP). It should be noted that the effect of friction reducers was not taken into account in these calculations.

3.3 Diverter Efficiency

A 12-stage slick water re-fracturing treatment was simulated. Each pumping stage includes 80 minutes of pumping at the rate of q = 60 bbl/min followed by a 20-minute pump break. Two cases were simulated: one with diverters and one without diverters. In the first model, which represents the case of fully effective diverters, two consecutive perforations, one old and one new, were plugged after each pumping cycle, moving from the heel toward the toe. In the second model, the effect of diverters was ignored and all perforations were left open to take fluid during all pumping stages. Figure 8 shows the flow rate and bottom-hole pressure graphs for both models.

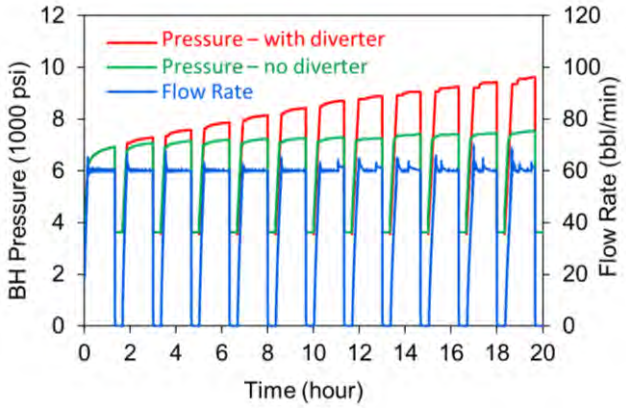

Figure 8: Flow rate and bottom-hole pressure plots for 12-stage re-fracturing simulations.

The increasing trend of treatment pressure in Figure 8 is consistent with the field observations in most re-fracturing cases; the treatment pressure rises after each pumping cycle during the treatment. This trend is usually interpreted as an indication of diverter efficiency. However, as Figure 8 shows, the pressure can rise (though probably to a lesser extent) even when no diverters are applied. In this case, the increase of treatment pressure would be related to the gradual increase of reservoir pressure during the treatment, which results in the progressive reduction of pressure gradient between the well and the reservoir. Under this condition, the injection pressure must be constantly increased in order to reach and maintain the design flow rate. The amount of pressure increase depends on several factors, including previous stage duration, pump break time, reservoir permeability, reservoir isolation, fluid viscosity, and other factors. For the simulated cases, the pressure increase for the case with no diverter was about 700 psi after 12 pumping stages; while for the case with diverter, it was 2,700 psi.

Figure 9 shows the evolution of the well pressure profile during the first 60 minutes of the first pumping stage. As the flow rate rises, the pressure profile diverges from the initially flat line and gradually becomes steeper until the target flow rate of 60 bbl/min is reached. After this point, the slope of the pressure profile remains almost constant during the rest of the stage. In this case, an injection pressure contrast of about 1,600 psi forms between the heel and the toe.

Figure 10 and Figure 11 show the perforation discharge profiles along the lateral at four stages of the treatment for the with-diverter and no-diverter models, respectively. In both cases, the discharge rate is initially higher at the heel and diminishes toward the toe, which is consistent with the higher well pressure developed at the heel and the lower pressure developed at the toe due to the frictional losses along the lateral (Figure 9). In the case of the with-diverter model (Figure 10) the discharge profile changes as more perforations are plugged off after each pumping stage; therefore, the high discharge front shifts gradually from the heel toward the toe. In the case of the no-diverter model, however, the discharge profile remains almost unchanged during all stages of the simulation.

In both cases, when the injection pressure exceeds the closure pressure on any pre-existing fracture, the fracture starts to dilate under the developed positive net pressure, resulting in a rapid increase in the fracture conductivity (fracture conductivity is proportional to the cube of fracture aperture). Given the higher well pressures closer to the heel, the pre-existing fractures in this region are more likely to dilate first (Figure 9). If diverters fail to plug off these dilated fractures at the heel, this condition persists throughout all stages of the treatment. This results in localized discharge of the fracturing fluid in this region, as shown in Figure 11.

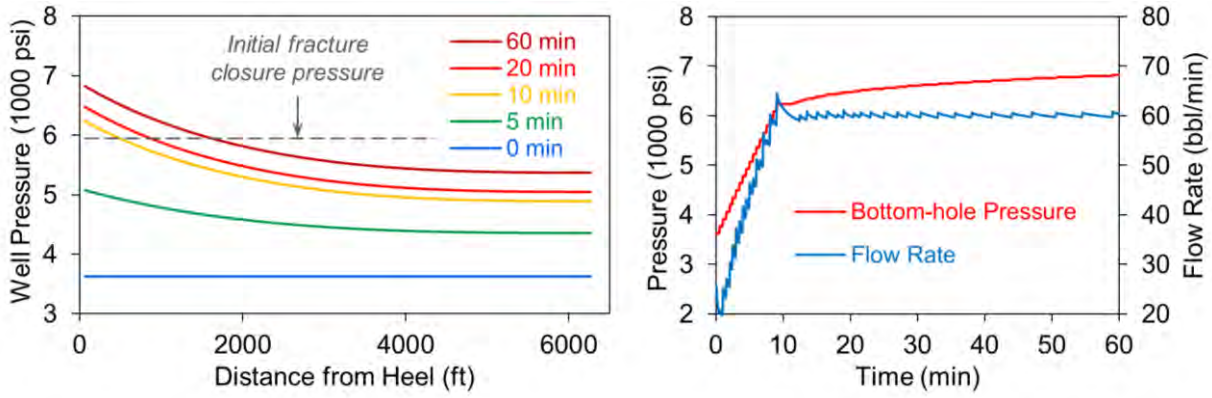

Figure 9: Evolution of pressure profile during the first 60 minutes of the first stage of the simulations. Pressure profile gradually becomes steeper as the flow rate increases until the target flow rate is reached. A pressure contrast of about 1,600 psi is developed under the constant flow rate of 60 bbl/min.

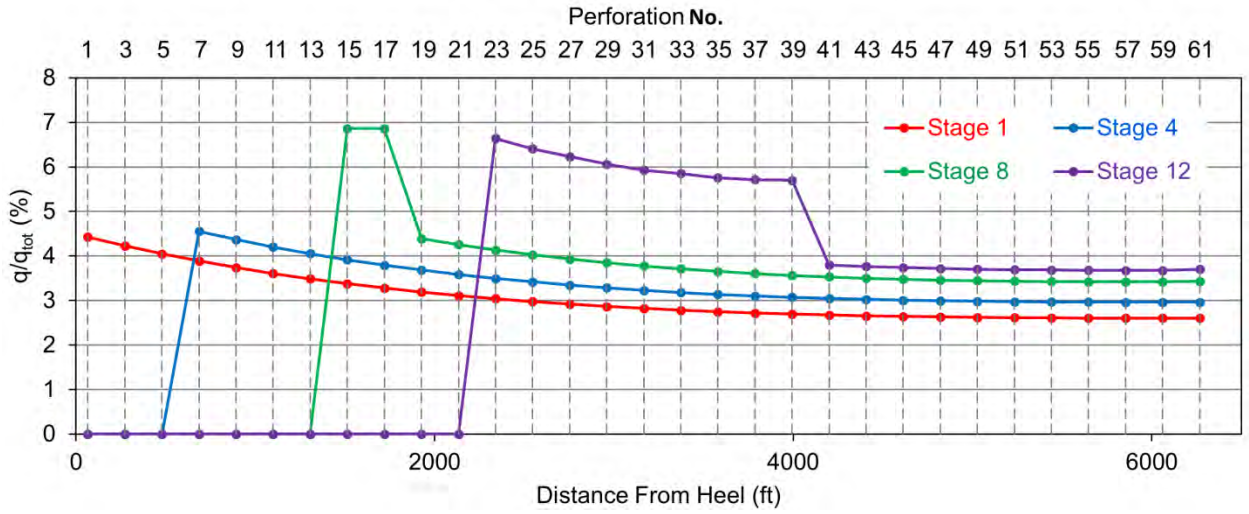

Figure 10: Perforation discharge profile (old perforations) for "with diverter" model at four stages of the treatment. The opening of pre-existing fractures under positive net pressure results in a sudden increase of the discharge rate on the associated perforations (first two open perforations in stage 8 and first nine open perforations in stage 12).

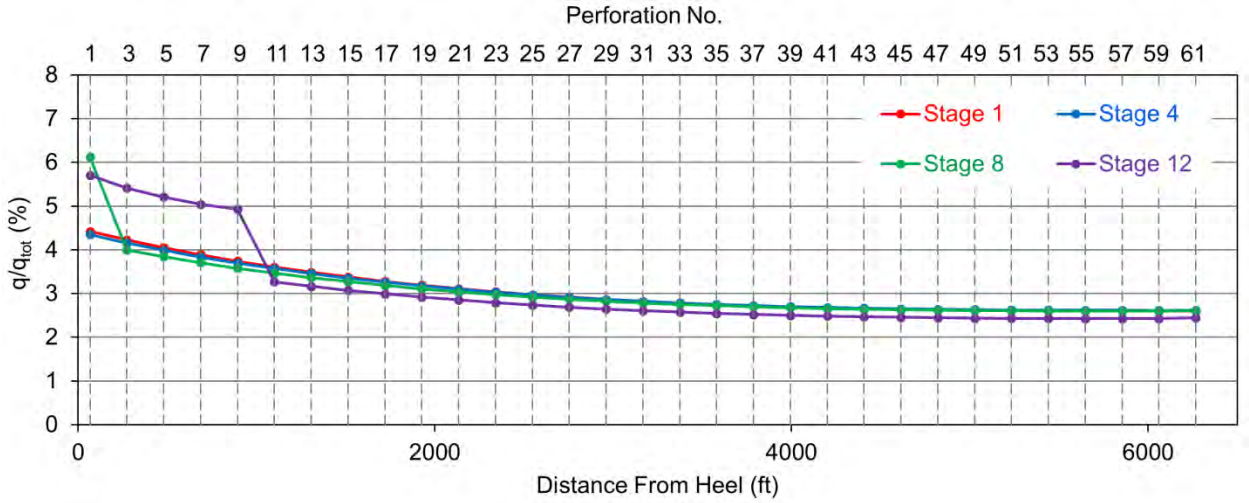

Figure 11: Perforation discharge profile (old perforations) for "no diverter" model at four stages of the treatment. The opening of pre-existing fractures under positive net pressure results in a sudden increase of the discharge rate on the associated perforations (first perforation in stage 8 and first five perforations in stage 12).

The synthetic microseismic events for both simulated cases are shown in Figure 12 and Figure 13. The synthetic microseismic event distribution for the no-diverter model matches closely with the field microseismic events recorded during re-fracturing of the studied wells shown in Figure 4. This similarity suggests that the diverters used for those treatments were not very effective in diverting the flow along the lateral, resulting in localized stimulation at the heel.

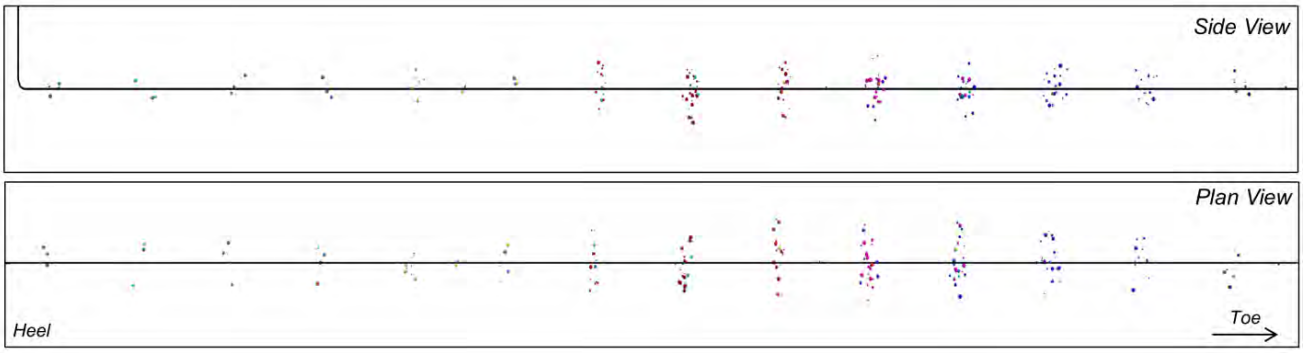

Figure 12: Synthetic microseismic events for the “with diverter” model. Only the first half length of the lateral (28 perforations) is shown.

Figure 13: Synthetic microseismic events for the “no diverter” model. Only the first half length of the lateral (28 perforations) is shown.

4 Geomechanics of Re-fracturing

4.1 Fracturing Versus Re-fracturing

There are several fundamental factors that make a re-fracturing treatment different from a fracturing treatment. The most important differences include:

- Altered stresses and pore pressures due to production.
- Pre-existing fractures, which provide paths of least resistance for the fluid.
- Altered permeability and flow capacity due to previous stimulations and production.
- Lack of mechanical isolation (for applicable cases).

Production has two major impacts on the reservoir stresses. First, during production the effective stresses rise on the rock matrix as the pore pressure depletes. Second, the higher effective stresses cause the deformation of the rock matrix, which results in the reduction of total stresses within the depleted zone. The extent to which the total stresses decrease during production depends on the pressure depletion ratio and the poro-elastic properties of the rock, i.e., Biot’s coefficient and modulus.

Figure 14 shows the stress and pore pressure contours after 1 month of production for a conceptual reservoir simulated numerically. It was assumed that the reservoir had been stimulated by hydraulic fracturing with initial stage lengths of 262 ft (80 m). The model parameters and the fracture characteristics are similar to those used for the re-fracturing models discussed in the previous sections. The contours show the ratio of the current state to the initial state for the

minimum effective stress (Sh'_{min}), minimum total stress (Sh_{min}), and pore pressure. The Mohr circles representing the full state of stresses at the well elevation are also shown.

After one month of production the Mohr circles representing the total stresses shift to the left (lower stress) while the circles representing the effective stresses shift to the right (higher stress). The change of the Mohr circle diameters during production indicate not only that the absolute magnitude of stresses change during production but so does the stress anisotropy. In this simulation a Biot's coefficient of α = 0.9 was considered.

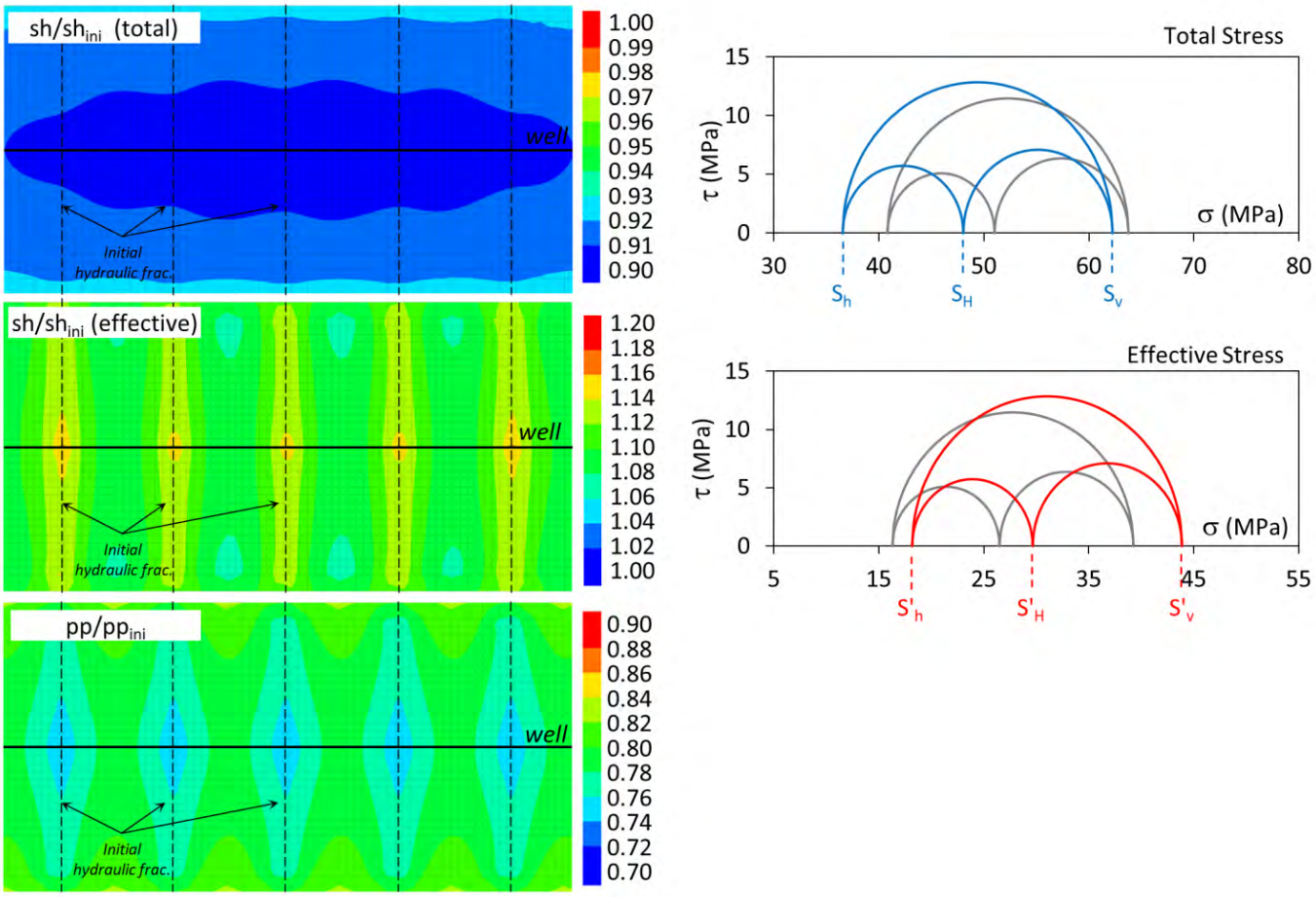

Figure 14: Numerical simulation of production in an initially stimulated reservoir. Contours show the ratio of current state (after 1 month of production) to initial state (before production) for total minimum stress (top), effective minimum stress (middle) and pore pressure (bottom). The Mohr circles (right) represent the full state of total and effective stresses before and after production

For re-fracturing, new perforations are usually added between the old ones in an effort to create new transverse fractures between the pre-existing fractures in order to enhance the fracture contact area within the reservoir. However, for a new fracture to initiate and propagate from the new perforations, three conditions must be met:

- Well pressure must exceed the available rock strength to initiate a new fracture (fracture initiation pressure or formation breakdown pressure).
- A positive net pressure (P_{net}=fluid pressure – Sh_{min}) must develop inside the fresh fracture in order to keep the fracture open.
- The treatment flow rate should exceed the flow capacity of the rock in order to inflate the

fresh fractures and to force them to propagate away from the wellbore

Old perforations, on the other hand, are already in hydraulic connection with the pre-existing fractures, and will open once the fluid pressure exceeds the total stress acting normal to their planes or Fracture Closure Pressure (FCP). This is shown graphically by the schematic mini-frac test graph in Figure 15. As shown in this figure, a higher pressure (equal to FBP) is initially required to overcome the rock strength and the near-wellbore effects, such as perforation friction and tortuosity, in order to breakdown fresh rock and initiate a new fracture. Once the fracture is initiated the pressure drops to the fracture propagation pressure (FPP), which is the pressure required to generate and maintain a positive net pressure to extend the fracture.

Conversely, in the case of pre-existing fractures, no formation breakdown is required. Once the well pressure reaches the FCP, the fractures start to open and take fluid until the pressure rises to FPP when the pre-existing fractures start to extend further. The difference between FBP and FCP is usually a few hundred psi for most formations.

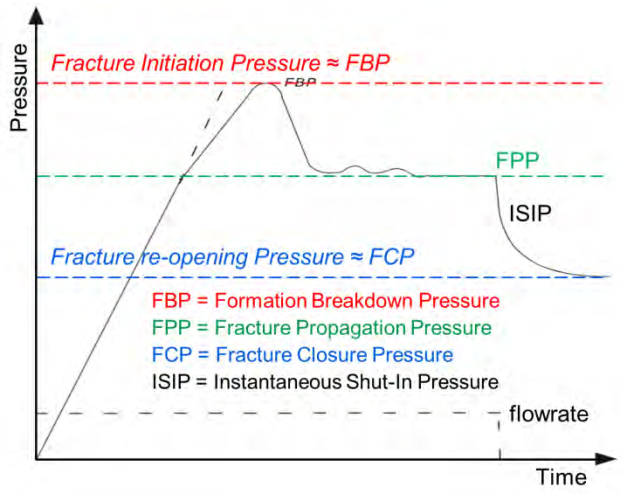

Figure 15: Schematic mini-frac pressure-time graph (*After Zoback M. 2010*).

It is important to note that the failure of fresh rock, or fracture initiation, is controlled by the effective stresses (total stress minus pore pressure), whereas the re-opening of pre-existing fractures is controlled by the total stresses; that is, they open once the fluid pressure developed inside the fractures exceeds the total stresses acting on their plane (usually Sh_{min}).

The effect of production on the reservoir stresses results in the increase of the effective stresses and the decrease of the total stresses along the lateral, as shown in Figure 14. Therefore, the production-induced stress changes make it more difficult for new transverse fractures to initiate from the new perforations (higher pressure is required) while making it easier for the pre-existing fractures to re-open during re-fracturing (lower pressure is required).

If no mechanical stage isolation is used during re-fracturing of a horizontal well, all perforations along the lateral are simultaneously exposed to the same well pressure (ignoring the pressure drop by frictional forces). Under this condition, it is very unlikely for a new transverse fracture to initiate and propagate between two pre-existing fractures, mainly because of the higher pressure required to break intact rock, i.e. FBP, than to re-open an already broken rock, i.e. FCP. After the start of pumping, as the well pressure increases, it first reaches the FCP of the formation (Figure 9), which results in re-opening or dilation of the pre-existing fractures. After this point, any further increase in the well pressure mainly results in further dilation of these pre-existing fractures and further increase of their hydraulic conductivity.

This argument is consistent with the low apparent ISIPs typically observed during early stages of re-fracturing compared to the original ISIPs for the same well (or pad) (Figure 16). This suggests that the recorded ISIPs during re-fracturing are more related to re-opening of the pre-existing fractures than creation of new hydraulic fractures. As

treatment continues, the build-up of pore pressure around the pre-existing fractures results in the increase of total stresses in the reservoir (reverses the production effect), which is reflected as progressively increasing apparent ISIP or treating pressure during re-fracturing (Figure 16).

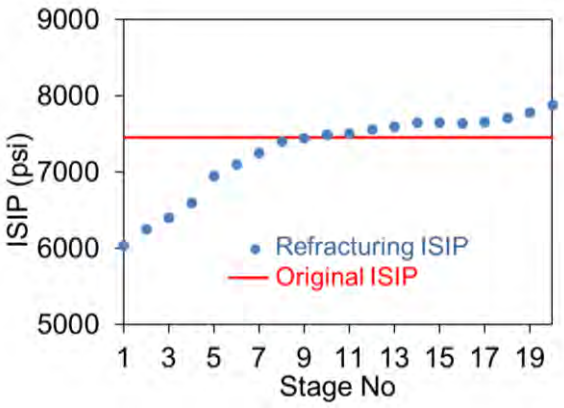

Figure 16: Apparent ISIPs (blue dots) for 20 stages of a re-fracturing treatment (well C in Figure 1). The red solid line shows the fresh rock ISIP recorded during the fracturing of the same well.

Another important factor in the design of a re-fracturing treatment is the applied injection rate relative to the flow capacity of the formation. A fracture will propagate if the injection rate into the fracture exceeds the flow capacity of the formation; Nagel N. (2015). In other words, a fracture will propagate if the total volume of injected fluid per unit of time is greater than the leakoff rate into the formation, enabling a fracture volume to be created inside the rock. If, at any point during pumping, this balance becomes negative, the fracture propagation will stop and the fracture will close down.

In most cases of re-fracturing in the Haynesville and Eagle Ford formations, the typical applied rates are 60–70 bbl/min, which is basically equal to the typical injection rates for initial fracturing of one treatment stage in these formations. If the injected fluid is taken by all perforations (usually more than two dozen) during re-fracturing, the effective flow rate for each perforation will be way below the flow capacity of the formation. This implies that even if we manage to initiate new fractures at the new perforations, there will not be enough flow rate (hydraulic energy) available to extend those fresh fractures between the two pre-existing fractures with high hydraulic conductivity.

The conclusions suggest that, in the absence of mechanical isolation, it is very unlikely that new transverse hydraulic fractures will be created and extended from new perforations during re-fracturing. This conclusion mainly applies to the more recent wells, where the initial stage lengths are usually shorter (<300 ft), making the well more uniformly stimulated and the pore pressure more uniformly depleted along the well. For longer initial stage lengths, which is usually the case in older wells, there is a better chance of developing new fractures from new perforations at less depleted intervals.

4.2 Dominant Stimulation Mechanism

Microseismicity is the acoustic representation of rock failure. When rock breaks, either in shear or in tension, the elastic strain energy stored in the rock is released and generates an elastic wave that is captured by the geophones and recorded as a microseismic event. Since the level of energy associated with the tensile failure of rocks is usually low during fracturing/re-fracturing (less than the sensitivity of the geophones), most of the microseismic events recorded during fracturing/re-fracturing treatments are shear events. The necessary conditions for shear failure of rocks are usually determined by using the Mohr-Coulomb failure criterion as follows:

$$\tau = c + \sigma_n' \tan \varphi \qquad (5)$$

where τ is shear stress, c is cohesion, σ_n' is the effective normal stress (total stress minus pore pressure), and φ is the internal friction angle.

Considering the Mohr-Coulomb's failure criterion, a shear failure will occur if any of the following conditions is met:

1. The stresses acting on a weakness plane change so the resulting shear stress exceeds the available shear strength (commonly referred to as “dry” microseismic events).
2. Pore pressure rises so that the available shear strength drops below the shear stresses acting on the weakness plane (commonly referred to as “wet” microseismic events).

The shear stimulation due to changes in stresses is mainly driven by the propagation of a new hydraulic fracture. Agharazi et al. (2013) and Nagel et al. (2014) showed that a high shear zone develops at the tip of a propagating hydraulic fracture, which moves with the propagating fracture tip. Natural fractures that fall inside this shear zone experience an increase in shear stresses and may slip, depending upon their orientation and shear strength characteristics. These failures are dry events since they are purely driven by stress changes (no fluid pressure change involved). Because these events are associated with the propagation of the hydraulic fractures, they are expected to be observed during the early minutes of pumping.

Behind the shear zone, a compressive zone forms on either side of the fracture with lower shear stresses, Agharazi et al. (2013) and Nagel et al. (2014). Within this region, the build-up of pore pressure due to fluid leakoff during the treatment is the only mechanism that can stimulate shear failure (wet events) on natural fractures.

During re-fracturing, however, no major fresh hydraulic fracture develops, as discussed in the previous section. Therefore, no major change of shear stress on natural fractures is expected. In this case, the dominant stimulation mechanism will be the pore pressure-driven shear slippage of natural fractures, which takes place due to the increase of reservoir pressure during re-fracturing. For this mechanism to be effective, the pore pressure must be raised to a critical level at which the available shear strength on weakness planes fall below the active shear stresses. This mechanism is graphically represented by shifting the Mohr circles toward the Mohr-Coulomb failure envelope (less effective stress), as shown in Figure 17.

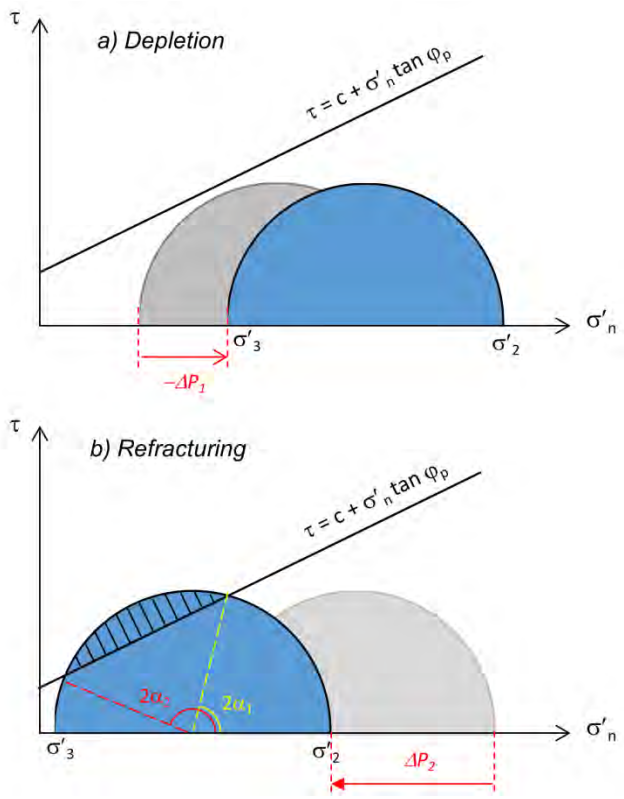

Figure 17: Mohr Circles schematically showing the variation of effective stresses on weakness planes during a) depletion and b) re-fracturing. By injecting the fluid during re-fracturing, the pore pressure on weakness planes increases by ΔP_2, resulting in failure of weakness planes oriented at angles between α_1 and α_2 (measured as the angle between normal to the plan and σ_2 direction).

Due to the low permeability of unconventional reservoirs and the prior pressure depletion caused by production, the build-up of pressure to the critical level is a lengthy process and usually takes several hours of pumping and several thousand barrels of slurry. This explains the frequently observed long delay in microseismic response to re-fracturing, as depicted in Figure 4, and the high volume of slurry injected into the

lateral during this time, as depicted in Figure 1 and Figure 3. This mechanism is also consistent with the observed increase of event count per pumping stage, as shown in Figure 3.

In a low permeability rock such as unconventional reservoirs, pore pressure can be increased in two ways;. first, directly by injecting high pressure fluid into the rock, and second indirectly by loading of the rock (undrained loading). In the second case, the pore pressure builds up due to rock deformation (poro-elastic effect), Jaeger et al. (2007), Detournay and Cheng (1993), Nomeli (2014). When the rate of loading (increase of net pressure on the fracture surface) is higher than the rate of pore pressure dissipation in the rock, the excess pore pressure generated by rock deformation cannot dissipate at the same pace as the rock (pores) deforms, resulting in the build-up of pore pressure. The level of pore pressure increase under such loading conditions depends upon several factors, including Biot's modulus, Biot's coefficient, the rate of loading. Given the nano-Darcy permeability of unconventional reservoirs, the common rate of loading in most fracturing treatments is high enough to generate some pore pressure in an indirect fashion.

This effect was numerically simulated for a single fracture with a height of 262 ft (80 m) and maximum length of 787 ft (240 m). The maximum net pressure (fluid pressure minus Sh_{min}) of 300 psi, acting at the fracture center, was applied over a course of 2 minutes. The maximum induced fracture width was measured as w_{max}= 13.8 mm at the fracture center. Figure 18 shows the pore pressure increase contours (ratio of current pore pressure to initial pore pressure) on a horizontal section crossing the center of the fracture. The illustrated pore pressure build-up is solely due to the inflation of the fracture under the applied load and does not include any leakoff effect.

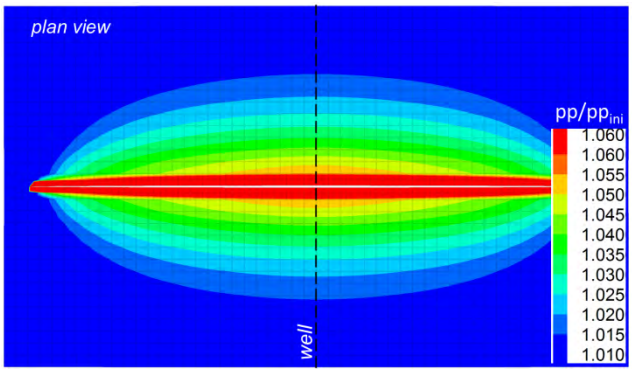

Figure 18: Excess pore pressure generated solely by the deformation of rock under a positive net pressure inside the hydraulic fracture (no leakoff involved). The contours represent the ratio of current pressure to the initial value for a fracture with maximum total length of 240 m. The maximum net pressure and width at the fracture center are 300 psi and 13.8 mm, respectively. (Mesh deformation exaggerated by a factor of 50).

5 An Optimized Re-fracturing Design

5.1 Two-Step Pumping Method

We developed and numerically examined an alternative re-fracturing method based on the microseismic observations and geomechanical studies described in the previous sections. The fundamental assumption of this method is that the dominant stimulation mechanism is the pore pressure-driven shear stimulation of natural fractures. Therefore, the treatment design mainly aims to increase the productive complexity within the reservoir. It also improves fluid conductivity of the pre-existing fractures.

The proposed method consists of two steps per pumping cycle, a slow pressurization step, during which pore pressure gradually builds up in the reservoir, followed by a stimulation step, during which high pressures are applied to initiate shear failures on critically stressed natural fractures (Figure 19).

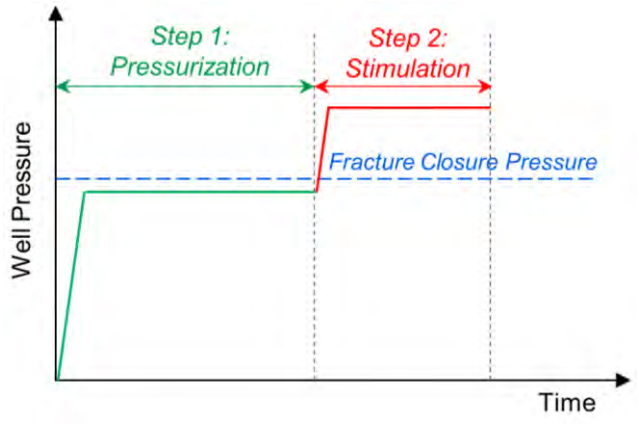

Figure 19: Schematic graph showing the treatment steps per pumping stage for the two-step re-fracturing method

During the first step, the fracturing fluid is injected into the well at a constant pressure, set just below the FCP of the formation. It is important to keep the injection pressure below FCP at this stage to avoid excessive dilation of the pre-existing fractures closer to the heel. The sole purpose of this step is to increase pressure in the reservoir in order to put more natural fractures at the critical stress state. Because no stimulation is intended during this stage, no proppant should be added to the fluid. Any proppant injected at this stage will increase the resistance to the flow and will minimize the extent of the pressurized zone.

The first step is considered complete when the rate of flow-rate drop under constant injection pressure becomes slow. Depending upon the reservoir permeability and pressure state, this stage can take up to a few hours. Longer pumping time and lower viscosity help to increase the extent of the pressurized zone at this stage. Note that pressure diffusion is inversely related to fluid viscosity, Jaeger et al. (2007).

Once the pressurization stage is complete, to switch to the next step, the injection pressure is increased until the target flow rate is reached. Very high flow rates should be avoided at this stage to keep the pressure drop rate low and to maintain a relatively uniform pressure profile along the lateral. Note that the pressure drop is proportional to the square of flow rate, so any small increase in flow rate will result in a considerable increase in the pressure drop rate [Equation (1)].

Proppant should be added to the slurry at this stage. Fluids with higher viscosities can be used to lower the flow rate while maintaining the high injection pressure during this stage. The minimum flow rate, however, should be selected by considering the proppant transport capability of the slurry in order to avoid early screen outs. Higher viscosity also shifts the pore pressure generation mechanism from flow-dependent (pressure diffusion) in step 1 to rock deformation-dependent (poro-elastic effect) in step 2.

Several pumping cycles should be performed to enhance the stimulation efficiency. The pump break time between the treatment cycles must be kept short to minimize the dissipation of the pore pressure generated during the previous pumping stages. Considering the increase of formation closure pressure with pore pressure, the injection pressure of step 1 must also be increased after each pumping stage.

5.2 Numerical Simulation

We numerically simulated one pumping stage of the proposed method. Two cases were studied. In the first case, slick water (SW) (μ = 2.5 cP) was injected during both steps. In the second case, slick water (μ = 2.5 cP) was injected during the first step and linear gel (LG) (μ = 20 cP) during the second step. Pump curves for both cases are shown in Figure 20.

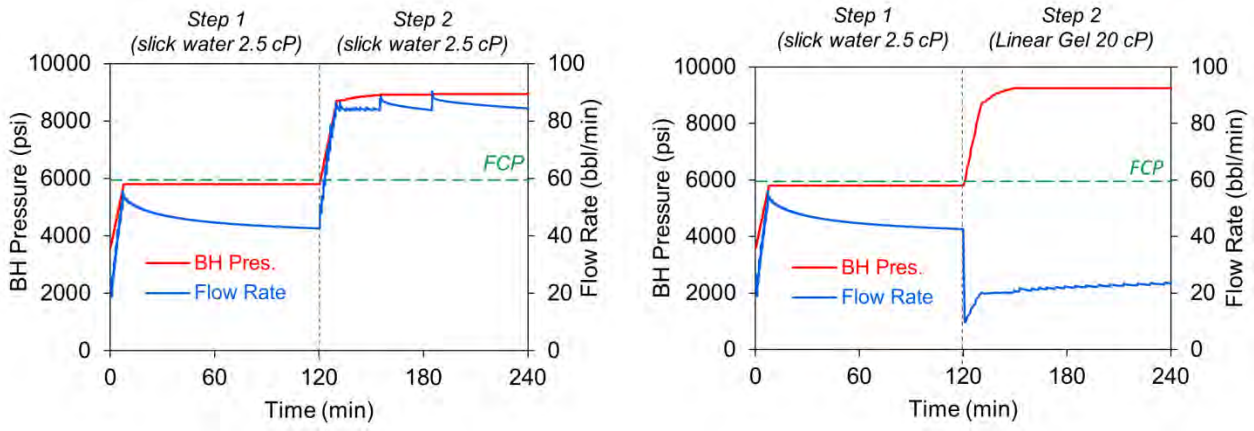

Figure 20: Bottom-hole pressure and flow rate graphs for the two-step re-fracturing numerical model. In both simulations slick water with viscosity of μ = 2.5 cP was used for the pressurization step. Two fluids were used for the second step. Slick water (left graph) and linear gel (μ = 20 cP) (right graph).

During the pressurization stage (step 1) the injection pressure was kept at P_w=5800 psi (40 MPa), just below the formation closure pressure *FCP*=5950 psi (41 MPa). The first step was complete after two hours, when the flow rate dropped to almost a constant value of q=43 bbl/min (Figure 20). The injection pressure was then increased to the design bottom hole pressure of P_w = 9200 psi to switch to the second step.

high pressure contrast developed along the lateral that led to a non-uniform discharge profile with high discharge rates at the heel. Increasing fluid viscosity at step 2 in the SW-LG model dropped the flow rate sharply, leading to uniform pressure and discharge profiles along the lateral. Note that no friction reducer was considered in these simulations. Adding friction reducer will lower the pressure contrast during the second step of the SW-SW model.

Figure 21 shows the pressure and discharge rate profiles for both models. In the SW-SW case a

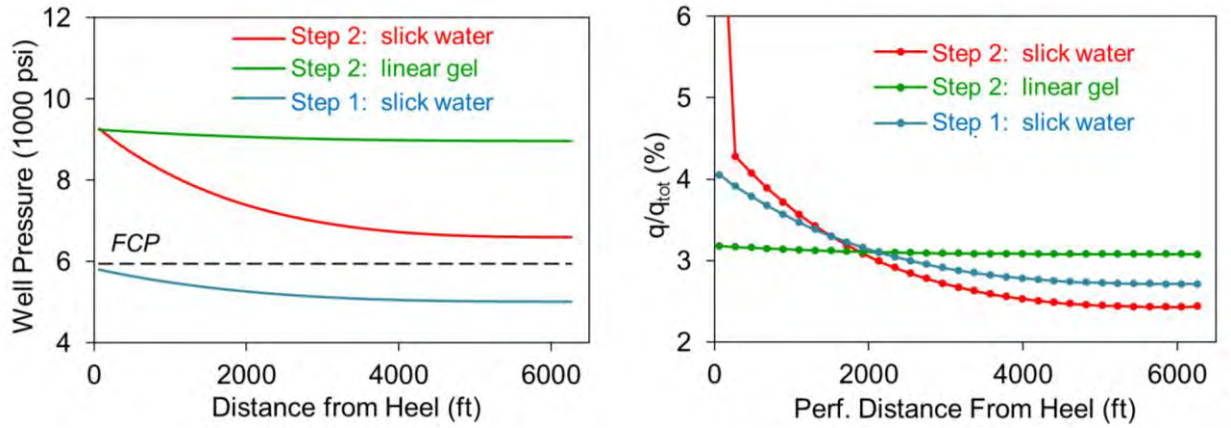

Figure 21: Well pressure (left) and discharge ratio (right) profiles for the simulated two-step cases: SW-SW and SW-LG.

The evolution of pore pressure on natural fractures during both stages of the treatment is shown in Figure 22 for the SW-LG case. The synthetic microseismic events associated with the

SW-LG model is also shown in Figure 23. As shown, a uniform microseismic event distribution developed along the lateral, indicating a uniform stimulation of the reservoir by the treatment.

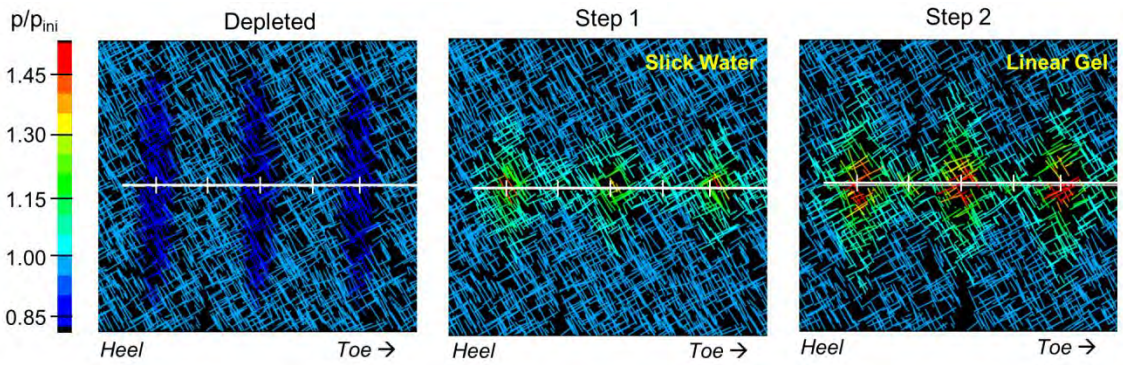

Figure 22: Evolution of pore pressure on natural fractures during the two-step SW-LG treatment simulation (just the first 600 ft of the well is shown).

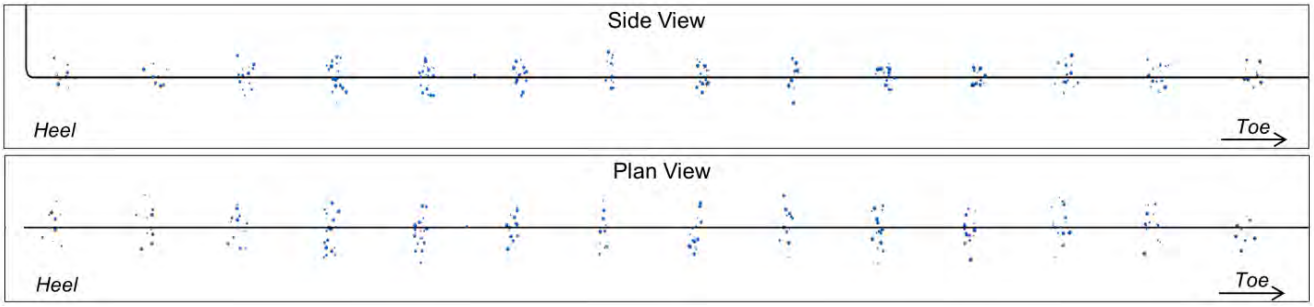

Figure 23: Synthetic microseismic events for the two-step SW-LG model (first half of the model is shown).

5.3 Best Candidates

Because the proposed method is based on shear stimulation of natural fractures by a pore pressure-driven mechanism, the following factors have a significant impact on the efficiency of the method and can be used as guidelines for selecting the best candidates for re-fracturing by this method:

- Stress anisotropy: Higher stress anisotropy increases active shear force on natural fractures, so less pore pressure is required to trigger failure.
- Fracture orientation relative to principal stresses direction: Assuming sub-vertical fractures, the most favorable orientation for shear failure is theoretically equal to $\beta=45-\varphi/2$ measured from s_{Hmax}, where φ is the friction angle of the fracture.
- Shear strength: Lower shear strength (lower c and φ) needs less pore pressure for shear failure to occur.

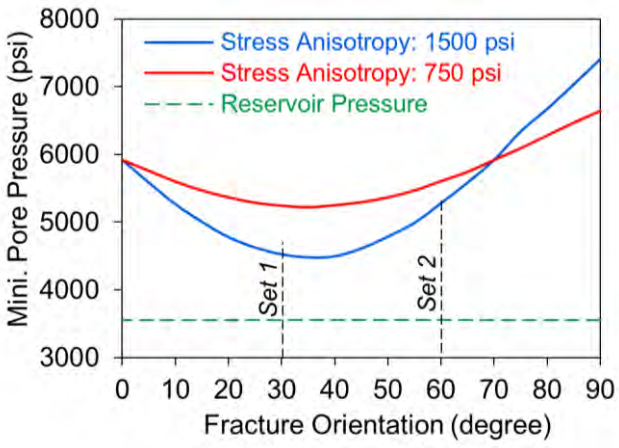

Figure 24: Variation of minimum pore pressure required to trigger shear failure on natural fractures for various sub-vertical fracture orientations. Two different horizontal stress anisotropies were considered. Dotted green line shows the reservoir pressure.

Figure 24 shows the minimum pore pressure required to trigger shear failure on sub-vertical fractures of various orientations. The stresses and pore pressures correspond to the values used in the numerical simulations. The minimum required pore pressure is calculated for two

stress anisotropies (S_{Hmax}- S_{hmin}) of 750 psi and 1500 psi. The graphs show how the required minimum pore pressure changes with the fracture orientation and stress anisotropy for a given fracture strength. It also shows that for reservoirs with originally higher pressure or those that are less depleted, it takes less pore pressure (energy) to trigger shear failure on natural fractures.

Considering the above factors the proposed two-step re-fracturing treatment method is more efficient in the over-pressure reservoirs, which are naturally fractured and have high stress anisotropy.

5.4 Design Requirements

The key factors in the success of the proposed re-fracturing treatment method are proper handling of injection pressures and flow rates with respect to the formation stresses and flow capacity, in order to avoid localized stimulation of the well at the heel. Therefore, accurate estimation of the reservoir pressures and stresses along the well is critical to the treatment success. Geomechanical models and numerical simulations can be used to calculate the current state of stress before re-fracturing, based on the pressure depletion data and the original reservoir stresses. The initial completion information provides a valuable source of data for this purpose. Due to the stress/pressure changes induced by the treatment in the reservoir, the injection pressures must be updated after each pumping cycle.

Considering the uncertainties in the field data and stress and pressure heterogeneities along the well, real-time adjustments to the design parameters must be considered. Real-time microseismic monitoring provides a powerful means for onsite assessment of the treatment parameters and applying the necessary adjustments as treatment continues.

A proper combination of treatment fluid and pumping rate must be selected to maintain a relatively uniform pressure profile during both steps of the treatment, while meeting the proppant transport requirements. The pressure drop must be calculated based on the well/casing specifications for each well.

6 Conclusion

In this study, we numerically modeled re-fracturing in a 6,400 ft long horizontal well with 61 perforations. The study showed that the main factors causing the concentration of microseismic events at the heel were i) pressure drop along the lateral due to frictional forces, and ii) inefficiency of the applied diverters.

Based on geomechanical principles we demonstrated that if no mechanical isolation is used, it is unlikely that a fresh hydraulic fracture from new perforations will be able to propagate between two pre-existing fractures. In this situation, the dominant stimulation mechanism is the shear stimulation of natural fractures by a pore pressure-driven mechanism.

Given the nano-Darcy permeability of unconventional reservoirs, it takes several hours of pumping and several thousand barrels of slurry to build up enough pore pressure within the reservoir to trigger shear failure of natural fractures, which explains the frequently observed delay in microseismic response to re-fracturing.

Based on these conclusions, we proposed an alternative re-fracturing method that consists of two steps per pumping stage. The basic principles of this method are:

- Pressurizing the reservoir before stimulation under an injection pressure lower than the formation closure pressure,

- Stimulating the reservoir under high injection pressure while keeping the flow rate low, to maintain uniform pressure and discharge profiles along the well.
- Repeating the same steps by running several pumping cycles and keeping the pump break time short.

The numerical simulations of the proposed re-fracturing method proved that the method was effective at generating a uniform stimulation pattern along the well, even with no diverters.

The proposed re-fracturing method aims at increasing the reservoir productive complexity and enhancing the hydraulic conductivity of the pre-existing fractures. Because the main stimulation mechanism is shear failure of natural fractures, the best candidate wells for this method are those in naturally fractured reservoirs that have a high stress anisotropy and high pore pressure.

Nomenclature

c	Cohesion
DFN	Discrete Fracture Network
FBD	Fracture breakdown pressure
FPP	Fracture propagation pressure
FCP	Fracture closure pressure
ISIP	Instantaneous shut-in pressure
LG	Linear gel
P_{net}	Net pressure acting on fracture plan
P_w	Bottom hole pressure
Sh_{min}	Minimum total horizontal stress
SH_{max}	Maximum total horizontal stress
Sv	Total vertical stress
Sh_{min}'	Minimum effective horizontal stress
SH_{max}'	Maximum effective horizontal stress
S_v'	Effective vertical stress
SW	Slick water
τ	Shear stress
φ	Internal friction angle
σ_n'	Effective normal stress

References

Agharazi, A., B. Lee, N. B. Nagel, F. Zhang, M. Sanchez. (2013). "Tip-Effect Microseismicity – Numerically Evaluating the Geomechanical Causes for Focal Mechanisms and Microseismicity Magnitude at the Tip of a Propagating Hydraulic Fracture". Presented at the SPE Unconventional Resources Conference Canada, Calgary, Canada, 5–7 November.

Detournay E., Cheng A. (1993). "Fundamentals of Poroelasticity". Online source: http://www.olemiss.edu/sciencenet/poronet/fundporo.pdf, (accessed November 01, 2015).

Diakhate M., Gazawi A., Barree B., Cossio M., Tinnin B., McDonald B., Barzola G. (2015). Refracturing on Horizontal Wells in the Eagle Ford Shale in South Texas – One Operator's Perspective". Presented at the SPE Hydraulic Fracturing Conference, The Woodlands, Texas, 3–5 February. SPE-173333-MS.

Jaeger J.C., Cook N.G.W., Zimmerman R.W. (2007). Fundamentals of Rock Mechanics. 4th Edition. Blackwell Publishing Ltd.

Lantz T.G., Greene D.T., Eberhard M.J., Norried R.S., Pershall R.A. (2007). "Refracture Treatments Proving Successful In Horizontal Bakken Wells; Richland Co, MT". Presented at the Rocky Mountain Oil & Gas Technology Symposium, Denver, Colorado, 16–18 April. SPE-108117-MS.

Munson B. R., Rothmayer A.P., Okiishi T.H., Huebsch W.W. (2012). Fundamentals of Fluid Mechanics. 7th Edition. Wiley

Nagel N. B., Sheibani F., Lee B., Agharazi A., Zhang F. (2014). "Fully-Coupled Numerical Evaluations of Multiwell Completion Schemes: The Critical Role of In-Situ Pressure Changes and Well Configuration". Presented at the SPE Hydraulic Fracturing

Technology Conference, The Woodlands, Texas, 4–6 February. SPE-168581-MS.

Nagel N. B. (2015). “Hydraulic Fracturing: Of Magic and Engineering”. Online source: https://www.linkedin.com/pulse/hydraulic-fracturing-magic-engineering-continued-neal-nagel?trk=prof-post (accessed November 08, 2015).

Nomeli, M.A., (2014). “Direct Numerical Simulation of Pore Scale Flow and Reactive Transport of CO2 in Porous Media”, American Geophysical Union, Fall Meeting, San Francisco, California , December 15-19, Abstract H11H-1012

Sudhendu K., Jbeili T. (2015). “Beating the decline through refracturing”. *World Oil Journal*, June 2015.

Vincent M. C. (2010). “Refracs – Why Do They Work, And Why Do They Fail in 100 Published Field Studies?” Presented at the SPE Annual Technical Conference and Exhibition, Florance, Italy, 19–22 September. SPE 134330-MS.

Zoback M. D. (2010). Reservoir Geomechanics. *Cambridge University Press*